JOURNAL OF MATERIALS SCIENCE 30 (1995) 1733–1741

# Structural and morphological evolution from a freeze-dried precursor to the $La_{1.85}Sr_{0.15}CuO_4$ superconductor during thermal processing

S. A. ALCONCHEL, M. A. ULLA, E. A. LOMBARDO
*Instituto de Investigaciones en Catálisis y Petroquímica, INCAPE (FIQ, UNL, CONICET), Santiago del Estero 2829, 3000 Santa Fe, Argentina*

The crystalline phases and morphology of solids with a composition of $La_{1.85}Sr_{0.15}CuO_4$ were studied in terms of thermal processing conditions of freeze-dried acetates. Samples were characterized by X-ray diffraction, scanning electron microscopy and iodometric titration techniques. Results indicate that a full development of the superconducting phase only occurs after pressing sintering and annealing under oxygen of the powders treated at $T_f = 1253$ K for 8 h. The structural evolution observed in this case involves a solid-state reaction between $La_{1.67}Sr_{0.33}Cu_2O_{5-\delta}$, $La(OH)_3$ and CuO. The existence of transient liquid phase at temperatures around 600 K generates local composition fluctations (lanthanum deficiency) where the non-superconducting ternary compound $La_{1.67}Sr_{0.33}Cu_2O_{5-\delta}$ develops. The selection of high heating rates (50 K min$^{-1}$) below 773 K minimizes the deleterious effect of transient melting and, at the same time, ensures a high reproducibility in the morphology of the final material obtained.

## 1. Introduction

The microstructure of high-temperature superconducting ceramics is critical, not only to the mechanical strength of these materials but also to their superconducting properties. Whereas the new superconducting ceramics have high critical temperatures and fields, their critical current densities are much smaller than required for most technological applications. There is now sufficient evidence to conclude that both the critical current density and the magnetic flux expulsion (Meissner effect) are strongly correlated to the microstructure of these materials. The key to the production of ceramics with adequate microstructure is the control of the starting powder characteristics.

We have shown in a previous publication [1] that the cryochemical processing of acetate solutions, used in the preparation of the superconducting compound $La_{1.85}Sr_{0.15}CuO_4$, guarantees the production of homogeneous molecularly dispersed precursors. Furthermore, this procedure allows an appropriate control of the synthesis variables such as concentration of the dissolved species and final drying temperature which affect the microstructure of the solid.

In principle, each particle of homogeneous freeze-dried powder may react to form the desired pure superconducting phase. This process should be conducted in an oxidizing atmosphere to avoid the copper loss caused by the sublimation of cuprous acetate [1]. However, the appearance of a transient liquid phase at temperatures around 600 K complicates matters. This phenomenon, inherent to the mechanism of decomposition of the copper acetate and the melting of strontium acetate, undoubtedly affects the quality of the final product. Owing to the diffusion of each species at different rates, a loss of homogeneity occurs with the concomitant variation of local composition.

A similar effect has been reported by several authors [2–6] in the synthesis of other superconducting phases, starting from freeze-dried or spray-dried precursors made up from nitrates, acetates and/or formates. The origin of the transient liquid phase has been attributed to the dissolution of the salts in their own residual hydration water or the low melting point of copper nitrate. This hypothesis is not justified, however, when using acetates or formates.

This work was designed to study the influence of synthesis variables such as heating rate, $\beta$, final temperature, $T_f$, and cooling rate, $V_c$ on the conversion of freeze-dried precursors to $La_{1.85}Sr_{0.15}CuO_4$. A battery of techniques, such as X-ray diffraction (XRD), scanning electron microscopy (SEM) and iodometric titration, were used to characterize the solids obtained. The ultimate goal was to find the relationship between intrinsic (melting) and extrinsic ($\beta$, $T_f$, $V_c$) variables of the synthesis procedure, on the one hand, and the phase evolution and microstructural features, on the other.

## 2. Experimental procedure

### 2.1. Sample preparation

The freeze-dried precursors were obtained from a water solution containing the desired proportion of

0022–2461 

lanthanum, strontium and copper acetates (total cation concentration: 0.23 and 0.11 mol $l^{-1}$). These solutions were instantaneously frozen and dried at subambient temperatures in a commercial freeze-drier. More details about the precursor preparation have been reported elsewhere [1].

The thermal reaction of the homogeneous precursors to produce the superconducting phase was carried out in a horizontal transparent quartz reactor (diameter 0.05 m, length 0.60 m). This could be operated either under vacuum (1.3 Pa) or under flow of nitrogen, oxygen or their mixture (artificial air) in variable proportions [7]. The reactor was heated by a cylindrical oven driven by a temperature controller–programmer. The temperature was controlled within $\pm$ 0.1 K in the ramps and $\pm$ 1 K in the plateaus.

Three different steps are distinguished in the heat treatment. First, the precursors were heated at variable rates from room to final temperature. Second, in all samples except A and B (Table I), this heating continued isothermally at $T_f$ for 8 h. Third, the solids were cooled at variable rates. The different cooling rates were obtained by either turning off the oven and leaving the sample inside (slow) or by quenching at room temperature (fast).

To prevent explosion in oxygen, due to the decomposition products of the acetates ($C_3H_6O$), air was used up to 893 K and then switched to pure oxygen, both at a flow rate of 400 ml(STP) $min^{-1}$.

The main preparation parameters which characterize the conversion of the precursors are summarized in Table I. Samples C–F were ground, pressed at 490 MPa for 6 min and formed into a disc shape of 12 mm diameter and 2–3 mm thick. These pellets were sintered under an oxygen flow (400 ml(STP) $min^{-1}$) at 1253 K for 12 h. The heating rate was 5 K $min^{-1}$. The solids were slowly cooled under oxygen keeping the reactor inside the oven. Finally, the pellets were annealed in oxygen at 773 K for 6 h and slowly cooled in the same atmosphere.

## 2.2. Sample characterization

The crystalline phases present in the calcined powders and the sintered samples were identified through their XRD patterns. They were obtained at room temperature with a Rich–Seifert (Model Iso-Debyeflex 2002) instrument, using Cu$K_\alpha$ radiation ($\lambda = 0.1542$ nm), a nickel filter and a scanning rate of 0.6° $min^{-1}$. To check the presence or absence of impurity phases, slower scans were performed (0.12° $min^{-1}$) in selected angular regions, saturating the signals belonging to the main phase.

The oxygen contents in powders C–F were calculated using the procedure given by Appelman *et al.* [8]. Triplicate measurements of each sample were made using 80 mg aliquots.

The SEM observations were aimed at (i) characterizing the morphology of samples A, C, $C_1$, and F (Table I) before grinding, (ii) describing the agglomeration level of sample C treated with different methods of grinding and dispersion, (iii) analysing the microstructural evolution of sample C following pressing, sintering and annealing under an oxygen flow.

The observations and micrographs were made in a Jeol (Model JSM-35C) microscope using accelerating voltages of 20–25 kV. The oxides in the form of agglomerates were glued to metallic sample holders using silver paint. Several different preparations were made with powder C combining ball milling and ethyl alcohol dispersion of the oxide followed by ultrasound treatment. Sintered pellets made of sample C were mechanically fragmented and glued to the metallic sample holder with silver paint. This preparation was made in such a way as to leave exposed the internal section of the fractures. All the preparations were covered by a thin film of gold for better image definition.

# 3. Results

## 3.1. X-ray diffraction patterns

After heating the freeze-dried precursor from 300 K to 893 K in 12 min (sample A), a low crystallinity solid made of $La_2O_2CO_3$ (PDF 23-320/322) [9] and CuO (PDF 5-0661, 41-254) was obtained (Fig. 1a). Increasing the temperature from 300 K to 1073 K in 48 min (Sample B) allows the incipient development of the superconducting phase $La_{1.85}Sr_{0.15}CuO_4$ (PDF

TABLE I Thermal processing of freeze-dried precursors[a]

| Sample | Final temperature (K) | Time (h) | Heating rate (K $min^{-1}$) | | Cooling rate (K $min^{-1}$) |
|---|---|---|---|---|---|
| | | | 300–773 K | 773–$T_f$ K | |
| A | 893 | [b] | 50 | 5 | 1 |
| B | 1073 | [c] | 50 | 5 | 1 |
| C | 1253 | 8 | 50 | 5 | 1 |
| $C_1$[d] | 1253 | 8 | 50 | 5 | 1 |
| D | 1253 | 8 | 50 | 5 | 24 |
| E | 1253 | 8 | 3 | 3 | 1 |
| F | 1253 | 8 | 3 | 3 | 24 |

[a] Atmosphere: to 893 K, flowing air; to *RT*, flowing oxygen.
[b] Heated from 300 K to 893 K in 12 min and cooled to room temperature.
[c] Heated from 300 K to 1073 K in 48 min and cooled to room temperature.
[d] Total cation concentration of starting solution 0.11 mol $l^{-1}$; all other solids, 0.22 mol $l^{-1}$.

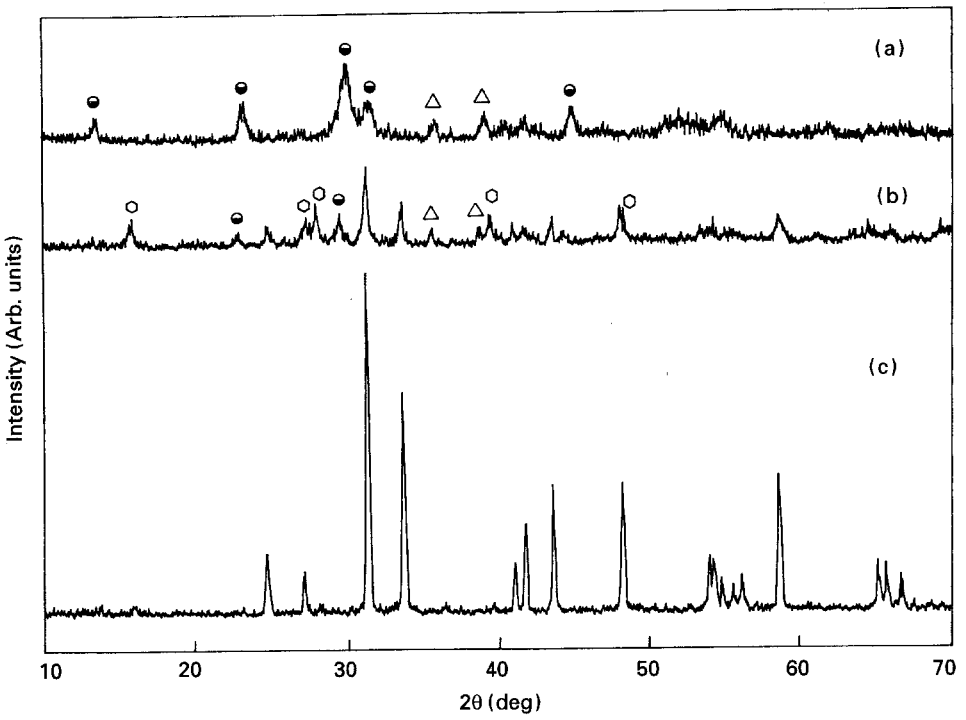


*Figure 1* XRD patterns of freeze-dried precursors after heat treatment at (a) 893 K in 12 min (Sample A), (b) 1073 K in 48 min (Sample B), and (c) 1253 K for 8 h (Sample C/$C_1$). More details in Table I. (◒) $La_2O_2CO_3$, (△) CuO, (○) $La(OH)_3$.

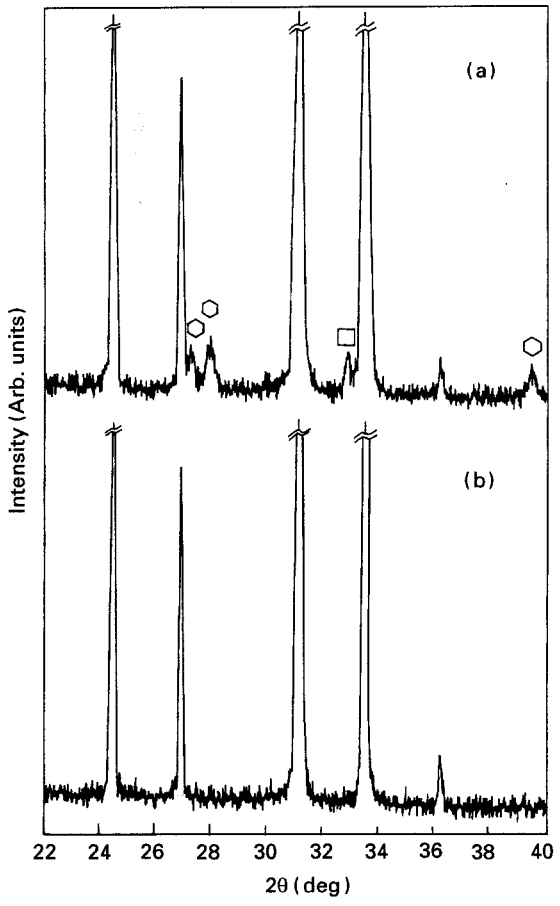


*Figure 2* Magnified XRD patterns of sample C ($C_1$). (a) Calcined powder (Table I) and (b) after sintering at 1253 K for 12 h and annealing at 773 K for 6 h, both in oxygen. (○) $La(OH)_3$, (□) $La_{1.67}Sr_{0.33}Cu_2O_{5-\delta}$.

39-1041). The signals appearing at $2\theta = 22.7°$, 29.4°; $2\theta = 15.6°$, 27.2°, 27.8°, 39.4°, 48.6° and $2\theta = 35.4°$, 38.6° are assigned to $La_2O_2CO_3$, $La(OH)_3$ (PDF 6-0585, 36-1481) and CuO, respectively (Fig. 1b).

The XRD patterns of samples C and $C_1$, heated at 1253 K for 8 h, show the presence of the superconducting phase with a $K_2NiF_4$ like structure as the major component (Fig. 1c). However, the presence of residual impurities was observed, which were identified as $La(OH)_3$ and $La_{1.67}Sr_{0.33}Cu_2O_{5-\delta}$ (PDF 39-1498) based upon the reflections observed at $2\theta = 15.6°$, 27.3°, 27.9°, 39.4°, 48.6° and $2\theta = 32.9°$, respectively.

These impurities are better seen in the patterns recorded in a magnified intensity scale and lower scanning rate (Fig. 2a). Sintering these materials followed by annealing in oxygen leads to monophasic oxides (Fig. 2b).

Similar results were obtained with samples D, E and F processed at the same final temperature ($T_f = 1253$ K) but with different combinations of β and $V_c$. $La_{1.85}Sr_{0.15}CuO_4$, $La(OH)_3$ and $La_{1.67}Sr_{0.33}Cu_2O_{5-\delta}$ were detected in the three samples. After sintering (1253 K) and oxygen annealing (773 K) the latter two phases disappeared from samples D and E (Fig. 3a and b) but not from F. The characteristic reflection, $2\theta = 32.9°$, of $La_{1.67}Sr_{0.33}Cu_2O_{5-\delta}$ is clearly seen (Fig. 3c).

## 3.2. Iodometric titration

The $y$ value in oxides C–F ($La_aSr_bCu_cO_y$) was calculated following the procedure given by Appelman

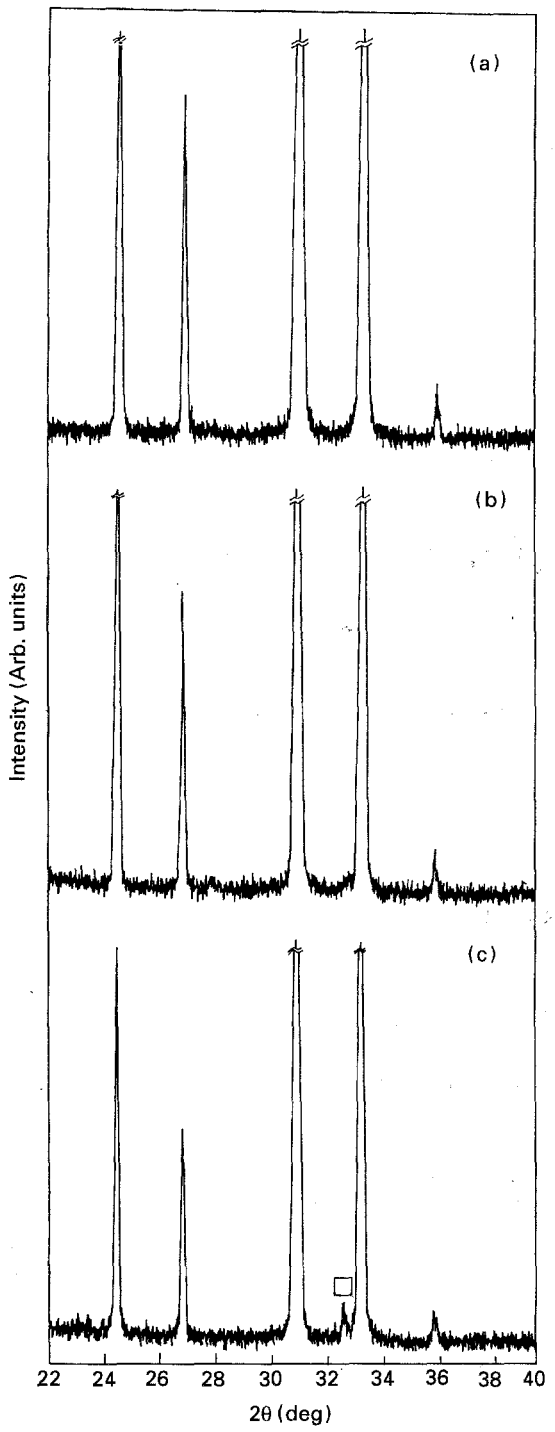


*Figure 3* Magnified XRD patterns of samples sintered and annealed as in Fig. 2b. (a) Sample D, (b) Sample E and (c) Sample F. (□) $La_{1.67}Sr_{0.33}Cu_2O_{5-\delta}$.

*et. al.* [8] based upon the ratio La:Sr:Cu = 1.85:0.15:1. The data obtained are reported in Table II.

TABLE II Oxygen content of $La_{1.85}Sr_{0.15}CuO_y$ powders obtained by iodometric analysis

| Sample | $y$ | $\bar{y}$[a] | S.D. | $\bar{y} \pm 3$S.D. |
|---|---|---|---|---|
| C | 3.9983<br>3.9983<br>3.9983 | 3.9983 | – | – |
| $C_1$ | 3.9983<br>3.9996<br>3.9983 | 3.9987 | 0.000 75 | 3.9987 ± 0.0023 |
| D | 3.9983<br>3.9971<br>3.9983 | 3.9979 | 0.000 69 | 3.9979 ± 0.0021 |
| E | 3.9933<br>3.9946<br>3.9946 | 3.9942 | 0.000 75 | 3.9942 ± 0.0023 |
| F | 3.9958<br>3.9958<br>3.9958 | 3.9958 | – | – |

[a] Mean value.

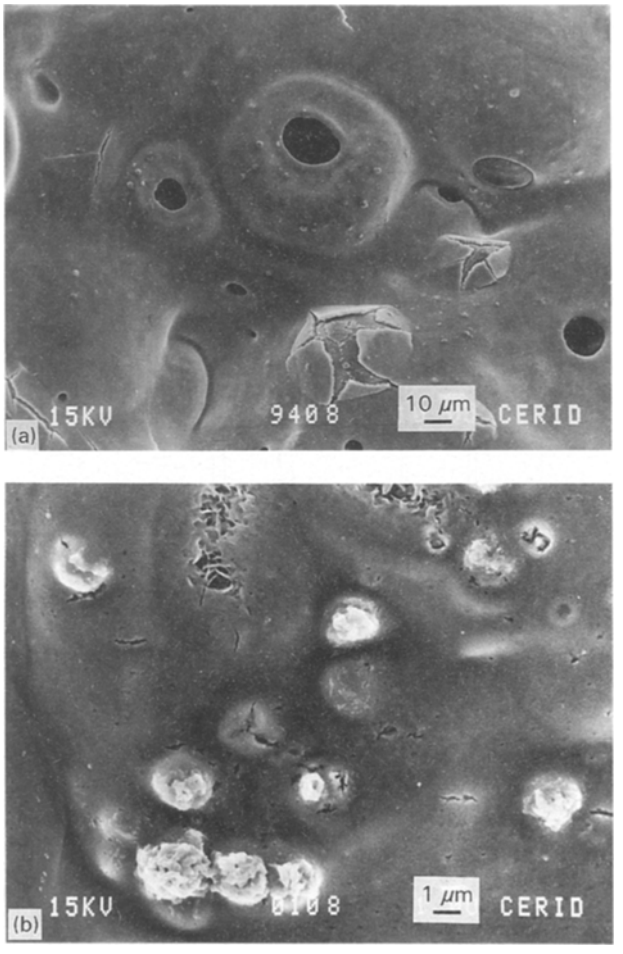


*Figure 4* (a) Irregular surface and (b) details of spheroidal microagglomerates of sample A ($T_f = 893$ K, $\beta = 50$ K min$^{-1}$, $V_c = 1$ K min$^{-1}$) before grinding (SEM).

## 3.3. Electron microscopy (SEM) observations

Samples A, C, $C_1$ and F were observed before grinding. A low-magnification view of sample A shows an irregular surface with globular formations and pores of varying size (Fig. 4a). Microagglomerates of ≈ 1 μm are also dispersed in this sample. At increasing magnification (Fig. 4b) it is seen that these emerging clusters are made up of aggregates of ≈ 0.1 μm. The spatial arrangement of these aggregates determines the spheroidal shape of the microagglomerates. The presence of cross-linked formations of ultrathin needles was observed less often.

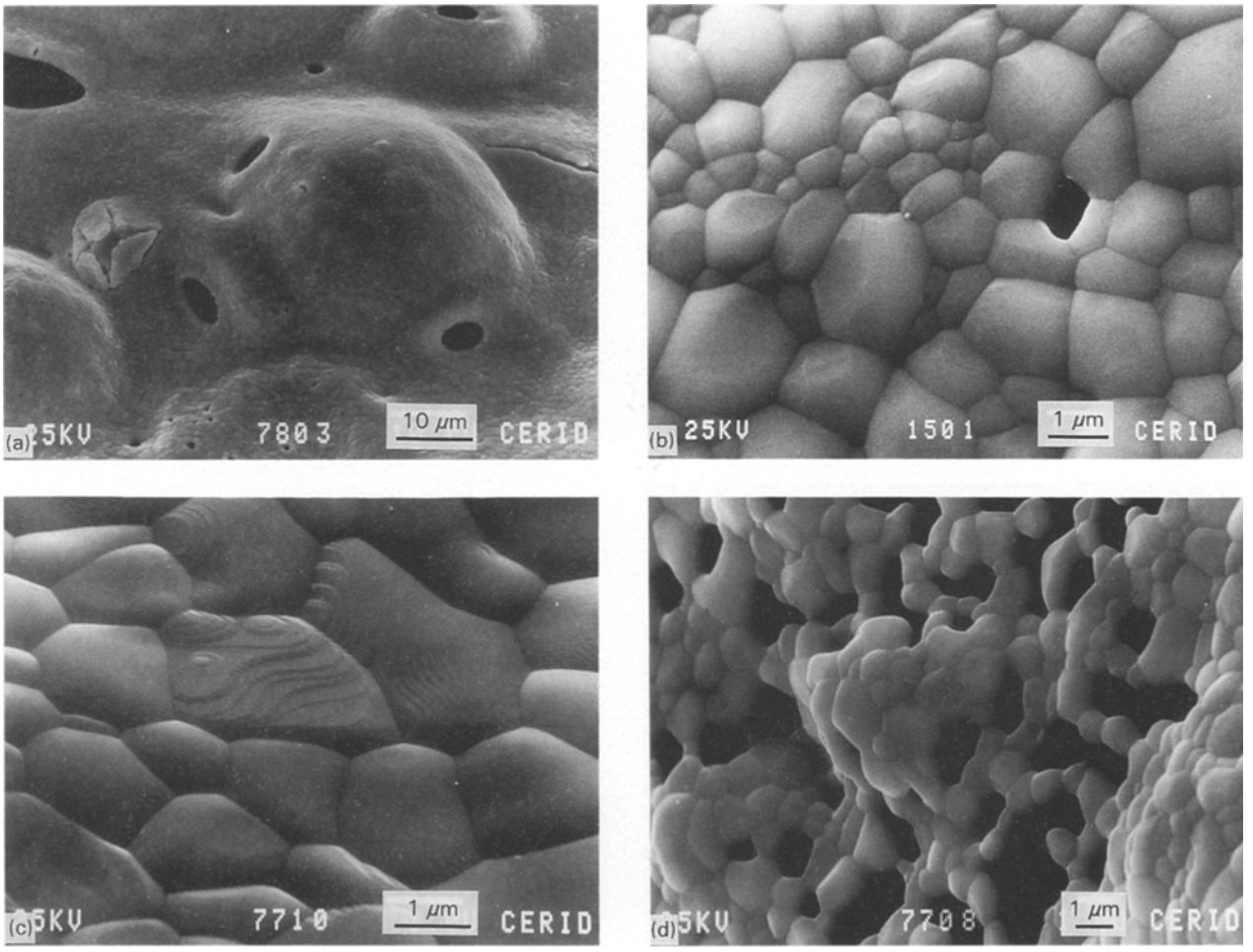


*Figure 5* Morphological features of sample C/C$_1$ ($T_f$ = 1253 K min$^{-1}$, $V_c$ = 1 K min$^{-1}$) before grinding. (a) Irregular surface, (b) packing of polyhedric grains, (c) growth layers or hillock, and (d) net-type structures.

The macrostructural features observed in samples C and C$_1$ are similar to those detailed above (Fig. 5a). The apparently smooth surface regions revealed, however, the granular structure seen in Fig. 5b. At increasing magnification (Fig. 5c) a high-density packing of polyhedric grains ( < 3 μm) is observed. Particularly, in the larger grains it is possible to see the presence of growth layers which may hint at the mechanism of grain enlargement during thermal treatment. Less often were net-type structures observed in some of the globules seen in the panoramic view (Fig. 5d). These structures showed a significantly higher concentration of pores originated by polyhedric grains ( < 1 μm) joined through faces and edges.

The morphology of sample F was quite different from the previous solids. Fig. 6a shows an overall view of this sample. In different regions the more regular surface contour was characterized by cracks and light and dark emission zones. The microstructure developed in the light regions (Fig. 6b) may be described as a matrix made up of grains with rounded edges of a size smaller than 0.5 μm. These formations with a highly homogeneous distribution of grain sizes, were also seen in the hillsides of the agglomerated solid. At higher magnification (Fig. 6c) the better defined grains are seen joined in the same manner as described in sample C. The dark areas are similar to the light ones except for a lower pore density and slightly longer grains.

The ground sample C may be described in terms of aggregates and agglomerates. The former are hard non-porous particles made up of crystallites held by high cohesive energy with size between 0.1 and 1 μm. The agglomerates are soft, somewhat porous clusters of aggregates with low cohesive energy, size > 1 μm [10]. The agglomerate size of the solids studied was smaller than 30 μm. Exceptionally, macroagglomerates of 100 μm were observed [7].

When the powders were dispersed in ethyl alcohol and treated with ultrasound for 20 min the typical size of the agglomerates was < 10 μm and with lower frequency there appeared larger clusters with a maximum size of 30 μm. Fig. 7a shows that most of these agglomerates are fragments of the material extracted from the reactor which are fractured at the grain boundaries. Spheroidal agglomerates of 5 μm composed of aggregates of 0.2 μm have been observed less frequently.

Ball milling the powder for 2 h followed by alcohol dispersion yielded bunches of aggregates, average size 0.2 μm, together with scattered larger formations up to 5 μm (Fig. 7b).

The observation of cross-sections of sintered pellets revealed the presence of areas of high and medium

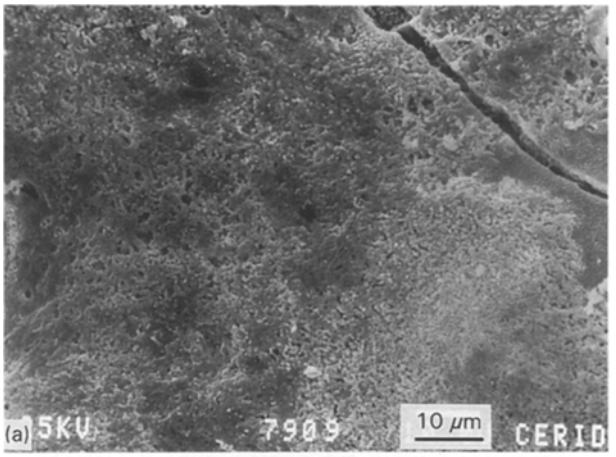


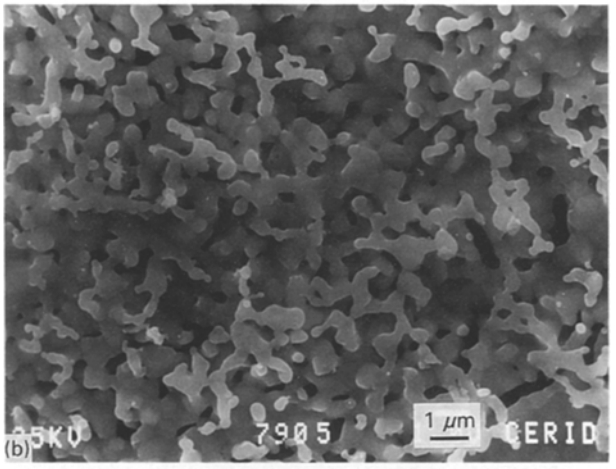


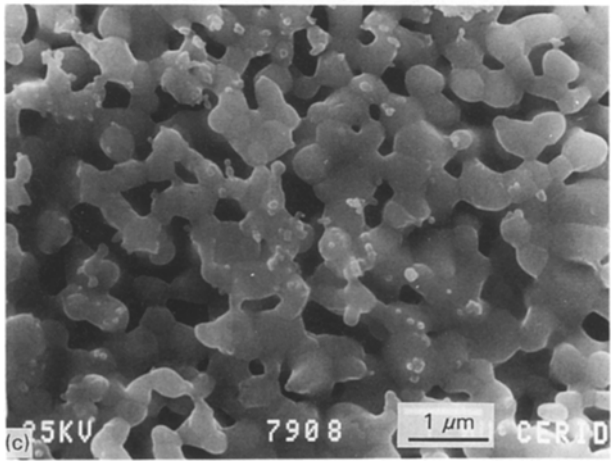


*Figure 6* Sample F ($T_f = 1253$ K, $\beta = 3$ K min$^{-1}$, $V_c = 24$ K min$^{-1}$) before grinding. (a) A more regular surface is evident than Fig. 5a. (b, c) Microstructural development in light regions.

density (Fig. 8a). The high-density region was associated with a significant increase in grain size with discontinuities as seen in Fig. 8b. On the other hand, the regions of intermediate density were characterized by the prevailing connection of small aggregates $< 0.5$ μm (Fig. 8c). Note the presence of pores originating through the interaction of three or four, or even more, aggregates. These clusters of grains showing uniform size distribution interact through their edges and faces. Another feature of the sintered pellets is the spheroidal shape of the smaller aggregates (0.2 μm).

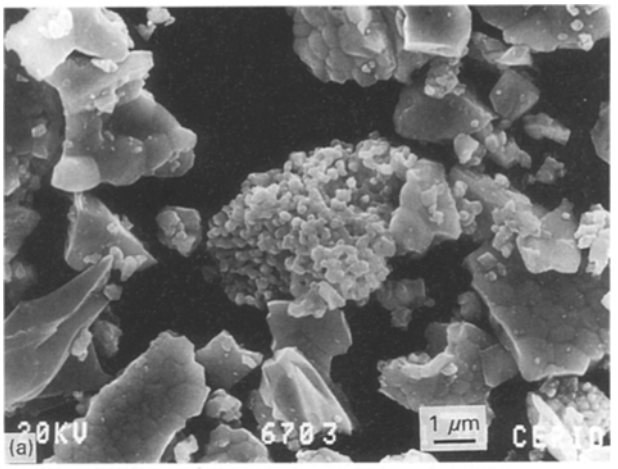


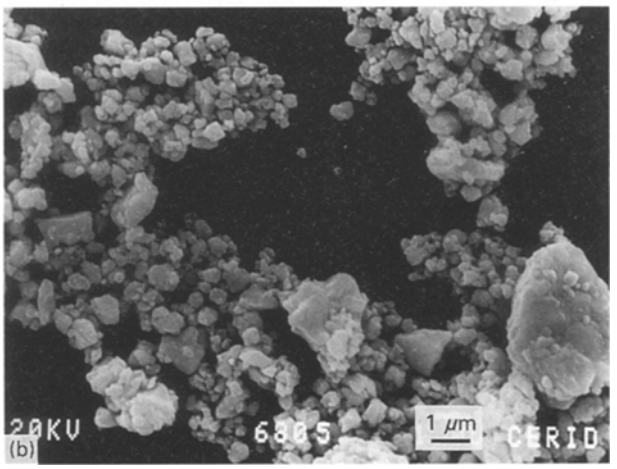


*Figure 7* State of agglomeration of powder C after (a) dispersing in ethyl alcohol and ultrasound treatment for 20 min, and (b) ball milling for 2 h followed by alcohol dispersion.

## 4. Discussion

### 4.1. Solid-state reactions and phase transformation

The changes occurring in the freeze-dried amorphous powder heated at temperatures between 893 and 1253 K were followed through the evolution of their X-ray diffraction patterns. When heated at 893 K in 12 min an incipient crystallization of $La_2O_2CO_3$ and CuO was observed (Fig. 1a). When the final temperature was increased to 1073 K, reached in 48 min, the superconducting phase became visible while the $La_2O_2CO_3$ has been partially converted to $La(OH)_3$ (Fig. 1b). The full development of the $La_{1.85}Sr_{0.15}CuO_4$ only occurs after pressing, sintering and annealing under oxygen of the powders treated at $T_f = 1253$ K for 8 h (Fig. 2). The phases observed in this case seem to indicate that the solid-state reaction occurring during sintering and annealing may be represented as follows

$$La_{2-z}Sr_zCu_2O_{5-\delta} + [2(1 + p)]\,La(OH)_3 + pCuO \rightarrow (2 + p)\,La_{2-y}Sr_yCuO_4 + [3(1 + p)]\,H_2O \quad (1)$$

where $p = z - y$.

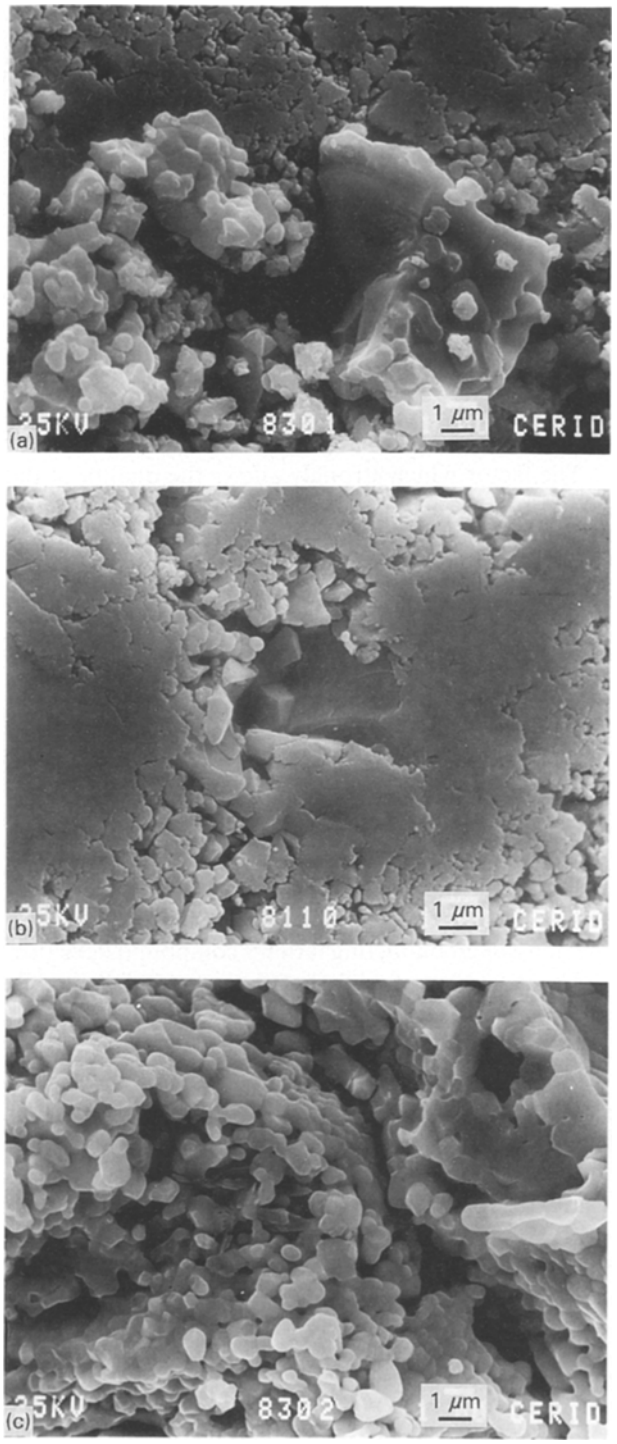


*Figure 8* Fracture surfaces of sample C sintered at 1253 K for 12 h and annealed at 773 K for 6 h, both in oxygen. (a) Representative view, and grain morphology in areas of (b) high and (c) medium density.

Payzant *et al.* [11] have reported that the presence of the non-superconducting oxide $La_{1.67}Sr_{0.33}Cu_2O_{5-\delta}$ is due to lanthanum deficiency during the solid-state synthesis of the $La_{1.85}Sr_{0.15}CuO_4$ phase. Accordingly, they suggested the following reaction scheme

$$[0.8577(2 - x)]La(OH)_3 + xSrCO_3 + CuO(O_2) \rightarrow$$
$$(A)\ La_{2-y}Sr_yCuO_4 + (B)\ La_{2-z}Sr_zCu_2O_5 +$$
$$xCO_2 + [1.2866(2 - x)]H_2O \quad (2)$$

where A and B vary with the amount of $La^{3+}$ required for the formation of the secondary phase.

This behaviour can also be explained in terms of the phase diagram of the system under study [12]. The co-existence of $La_{8-x}Sr_xCu_8O_{20-\delta}$ ($La_{2-z}Sr_zCu_2O_{5-\delta}$) in equilibrium with the superconducting phase, requires lanthanum compositions below the nominal value and also implies the presence of CuO.

In a previous contribution [1] it has been shown that the global stoichiometry of the freeze-dried powders is appropriate for the synthesis of $La_{1.85}Sr_{0.15}CuO_4$. Thus the origin of spurious phases might be related to the transient melting observed during the thermal decomposition of the precursor. The presence of liquid is likely to generate local inhomogeneities due to the different diffusivities of each species. The development of regions with lanthanum deficiency would favour the formation of the non-superconducting solid.

This may explain why using low heating ($3\ K\ min^{-1}$) and high cooling rates ($24\ K\ min^{-1}$) it is not possible to obtain a single-phase sintered solid (Fig. 3c), i.e. low $\beta$ values would increase the concentration gradients due to different diffusivities. This mass-transport effect would be reflected in the kinetics of Reaction 1 and, consequently, would diminish the conversion to the superconducting phase. Thus, the presence of the non-superconducting phase in the sintered sample F is a direct consequence of the thermal history of the starting powder.

## 4.2. Oxygen stoichiometry

The $y$ values calculated from iodometric titration are in line with the previous analysis. Table II shows that there is no statistically significant difference between the $y$ values obtained for the C, $C_1$ and D samples prepared with $\beta = 50\ K\ min^{-1}$. The oxygen content measured in these samples exactly corresponds with the values reported for the superconducting phase [8]. Note that both the proportion of impurities ($La(OH)_3$ and $La_{1.67}Sr_{0.33}Cu_2O_{5-\delta}$) and the cooling rate (1 and $24\ K\ min^{-1}$) do not affect the value of $y$.

On the other hand, a decrease in oxygen content was observed in oxides E and F which were obtained with $\beta = 3\ K\ min^{-1}$ and $V_c = 1$ and $24\ K\ min^{-1}$, respectively. This finding may be rationalized in terms of a lower conversion to the superconducting oxide as indicated by the X-ray diffraction patterns.

In calculating $y$, it is assumed that all of the sample analysed is the superconducting oxide. The existence of $La(OH)_3$ and CuO does not affect the consumption of titrating agent, but the $La_{1.67}Sr_{0.33}Cu_2O_{5-\delta}$ reacts with HBr, used to dissolve the solids, increasing the consumption of $Na_2S_2O_3$. Depending on the concentration of this ternary compound, the value of $y$ will increase.

In the powders analysed, it may be that the results obtained are due to a combination of variables, where the effect caused by the fraction of the superconducting phase ( $< 100\%$) in the solid prevails.

### 4.3. Morphology

Fig. 4a clearly shows the melted appearance of a fragment of sample A. The presence of globules and macropores is due to the abrupt expulsion of the decomposition products of the acetates. The resulting morphology, which originates in the sudden emission of gases trapped in a high-viscosity fluid, confirms the melting of freeze-dried powders previous to the thermal decomposition. The surface details seen in Fig. 4b, characterized by the presence of microagglomerates dispersed in the melted material, fits well with the segregation of phases at low calcination temperature (893 K) seen in the X-ray diffraction pattern.

Significant differences in microstructure were observed in samples C and $C_1$ compared to F, which are markedly dependent on the synthesis parameters. For $\beta = 50\ K\ min^{-1}$, $T_f = 1253$ K and $V_c = 1\ K\ min^{-1}$ (C and $C_1$) the dense packing of polyhedric grains, less than 3 μm in size, (Fig. 5b and c) reflects the sintering of melted oxides.

The pyramid (or hillock) structures observed in the large grains are similar to those described by Sun *et al.* [13] in single crystals of YBCO grown using the CuO-flux technique. These structures result from the interaction of many screw dislocations according to the growth mechanism advanced by these authors. The circular spiral morphology was associated with a high temperature of formation and indicates that the spiral steps can advance independently of the crystallographic directions.

These growth features were not seen in sample F ($\beta = 3\ K\ min^{-1}$, $T_f = 1253$ K and $V_c = 24\ K\ min^{-1}$). The limited grain growth observed in this solid (Fig. 6c) coincides with the morphological observations of Marella *et al.* [14] in platelets grown from partially melted bulk $YBa_2Cu_3O_{7-\delta}$. They observed that low cooling rates ($1\ K\ h^{-1}$) lead to the formation of large grains with preferential growth along the *c*-axis. Accordingly, they suggested a screw dislocation growth mechanism along the *c*-axis similar to that observed in epitaxially grown thin films and single crystals grown using the flux method. The model of screw dislocation growth predicts an increase in the fraction of preferred growth sites with undercooling and of the growth rate with the square of the undercooling [15]. This is one possible way of explaining why, by increasing the cooling speed, the grain growth is limited (Fig. 6c).

On the other hand, Reynen [16] has suggested that the presence of secondary phases, particularly when they are highly dispersed in the solid, drastically affects the sintering process. These intergrain phases play a role similar to grain boundaries but with lower mobility. Its conversion involves mass transport processes over longer distances, retarding the grain growth. This behaviour might also explain the microstructure seen in sample F.

The microstructure of the sintered sample C reveals a low sinterability of the original powder. The surface of fractures were characterized by high and medium density regions which were associated to a discontinuous grain growth (Fig. 8b and c). This behaviour might be due to density gradients generated during pellet formation at 490 MPa. Increasing this pressure to 880 MPa was not beneficial either, due to the fracture of the pellets that invariably occurred. This effect may indicate that the macroagglomerates present in sample C are not easily deformable because they come from a partially sintered material.

## 5. Conclusion

The synthesis of $La_{1.85}Sr_{0.15}CuO_4$ through thermal decomposition of freeze-dried precursors, involves several reactions which include CuO, $La_2O_2CO_3$, $La(OH)_3$, $La_{1.67}Sr_{0.33}Cu_2O_{5-\delta}$ and probably a strontium intermediate compound.

The factor which strongly affects the quality of the final product is the existence of a transient liquid phase at temperatures around 600 K. Its presence is inherent in the mechanism of thermal decomposition of copper acetate and the melting of strontium acetate before decomposition.

This effect induces phase segregation due to varying diffusivities of the intervening species. This loss of homogeneity introduces mass-transport limitations in the overall kinetics of the synthesis process. This phenomenon leads to two undesirable side effects: (i) the impossibility to decrease the synthesis temperature, $T_f$, which was expected from the use of the cryochemical method; (ii) the local composition fluctuations seem to generate lanthanum-deficient regions where the non-superconducting ternary compound develops.

The selection of high heating rates ($50\ K\ min^{-1}$) below 773 K has allowed us to minimize the deleterious effect of the transient melting and, at the same time, achieve a high reproducibility in the morphology of the materials obtained.

Despite these difficulties, it is possible to obtain monophasic oxides in the form of sintered pellets using powders calcined at 1253 K. The structural evolution observed in samples prepared under these synthesis conditions is consistent with the solid-state Reaction 1, which defines the final conversion stage to the superconducting oxide.

## Acknowledgements

This work was supported by a grant from CONICET PID 3-0956/88. The authors also thank Professor N. Pratta for her assistance with the scanning electron microscopy, Professor Elsa Grimaldi for her assistance with the English version, and the Department of Biological Chemistry for making the freeze-drying apparatus available.

## References

1. S. ALCONCHEL, M. ULLA and E. LOMBARDO, *Mater. Sci. Engng* **B** (in press)
2. S. JOHNSON, M. GUSMAN, J. ROWCLIFFE, T. GEBALLE and J. SUN, *Adv. Ceram. Mater.* **2** (1987) 337.
3. H. MEDELIUS and D. ROWCLIFFE, *Mater. Sci. Eng.* **A109** (1989) 289.
4. C. LACOUR, F. LAHER-LACOUR, A. DUBON, M. LAGUES and Ph. MOCAËR, *Phys. C* **167** (1990) 287.
5. J. BLOCK and L. DOLHERT, *Mater. Lett.* **11** (1991) 334.

6. K. TAKAHASHI, T. ITO, H. YOSHIKAWA and A. HIRAKI, *Jpn J. Appl. Phys.* **32** (1993) L1211.
7. S. ALCONCHEL, PhD thesis, Universidad Nacional del Litoral, Santa Fe, Argentina (1993).
8. E. APPELMAN, L. MORSS, A. KINI, V. GEISER, A. UMEZAWA, G. CRABTREE and K. CARLSON, *Inorg. Chem.* **26** (1987) 3237.
9. Powder Diffraction File, JCPDS (International Center for Diffraction Data, Swarthmore, 1991).
10. J. HEINTZ, F. WEILL and J. BERNIER, *Mater. Sci. Eng.* **A109** (1989) 271.
11. E. PAYZANT, H. KING and J. WALLACE, *Solid State Commun.* **76** (1990) 409.
12. D. De LEEUW, C. MUTSAERS, G. GEELEN and G. LANGEREIS, *J. Solid State Chem.* **80** (1989) 276.
13. B. SUN, K. TAYLOR, B. HUNTER, D. MATTHEWS, S. ASHBY and K. SEALY, *J. Crystal Growth* **108** (1991) 473.
14. M. MARELLA, G. DINELLI, B. BURTRET FABRIS and B. MOLINAS, *J. Alloys Compounds* **189** (1992) 123.
15. W. KINGERY, H. BOWEN and D. UHLMANN, (eds) in "Introduction to Ceramics" (Wiley, New York, 1976) p. 340.
16. P. REYNEN, private communication.

*Received 28 March*
*and accepted 7 September 1994*